CCFE
CULHAM CENTRE FOR FUSION ENERGY

UK Atomic Energy Authority

UKAEA-CCFE-PR(24)207

J. R. Harrison, C. Bowman, J. G. Clark, A. Kirk, B. S. Patel, P. Ryan, R. Scannell, A. J. Thornton, K. Verhaegh

Benefits of the Super-X Divertor Configuration for Scenario Integration on MAST Upgrade

Benefits of the Super-X Divertor Configuration for Scenario Integration on MAST Upgrade

J. R. Harrison, C. Bowman, J. G. Clark, A. Kirk, B. S. Patel, P. Ryan, R. Scannell, A. J. Thornton, K. Verhaegh

This is a preprint of a paper submitted for publication in Plasma Physics and Controlled Fusion

Benefits of the Super-X Divertor Configuration for Scenario Integration on MAST Upgrade

J. R. Harrison[1], C. Bowman[1], J. G. Clark[1], A. Kirk[1], J. Lovell[2], B. S. Patel[1], P. Ryan[1], R. Scannell[1], A. J. Thornton[1], K. Verhaegh[1]

[1] United Kingdom Atomic Energy Authority, Abingdon, Oxon, UK
[2] Oak Ridge National Laboratory, Oak Ridge, USA

E-mail: James.Harrison@ukaea.uk

Received xxxxxx
Accepted for publication xxxxxx
Published xxxxxx

Abstract

The integration of good core and edge/pedestal confinement with strong dissipation of heat and particles in the divertors is a significant challenge for the development of fusion energy. Alternative divertor configurations offer potential advantages by broadening the operational space where a device can operate with detached divertors and acceptible power exhaust. First results from MAST Upgrade are presented from high confinement mode experiments with outer divertors in the Super-X divertor configuration, showing that the outer divertors naturally detach when the Super-X is formed with no discernible impact on the plasma core and pedestal. These initial findings confirm predicted benefits of the Super-X configuration in terms of facilitating scenario integration.

Keywords: term, term, term

1. Introduction

The development of high-performance plasma scenarios in magnetic confinement fusion devices necessitates stable and favourable confinement in the plasma core (including thermal and energetic particles) and edge/pedestal regions and acceptible power exhaust. While the required levels of performance in each aspect vary between devices (e.g. ITER [1, 2] and DEMO [3, 4, 5]), a key aspect is the compromise between core and edge/pedestal confinement and power exhaust. It has been widely observed that dissipation of power and particles in the divertors can degrade confinement in the core and edge (e.g. [6, 7, 8] and references therein). Conversely, the achievement of good core and pedestal confinement can exascerbate the challenge of handling power and particle exhaust (e.g. [9, 10, 11]).

The development and study of integrated plasma scenarios that minimise trade-offs beween performance of the confined plasma and power exhaust is a very active area of research, with solutions broadly falling into three categories. Firstly, radiating impurities have been used in devices with conventional divertor configurations to dissipate a significant proportion of the power crossing the sepatrix before it reaches the divertors [12, 13, 14, 15], sometimes in combination with improved core confinement regimes [16, 17]. Secondly, alternative divertor configurations are employed to decrease the divertor heat flux via a combination of spreading the heat flux over a larger surface area and promoting dissipation of particles, momentum and energy in the divertor to promote access to the detached divertor regime [18, 19]. Finally, novel materials are being developed to withstand higher sustained heat fluxes (e.g. [20]) to help ease the constraints power exhaust places on scenario integration.

MAST Upgrade is an excellent facility for studying the comparative benefits of alternative divertor configurations in a low aspect ratio tokamak [21]. The device has significant

flexibility to independently vary the shaping of the plasma core and divertor configuration, and is optimised to study the Super-X divertor configuration [22]. The Super-X configuration is characterised by placing the outer strike points at large major radius and a region of low poloidal field along the outer divertor legs to increase the length of field lines connecting the outer mid-plane and outer divertor strike points. These characteristics of the Super-X are predicted to decrease the outer divertor heat flux via situating the strike points at lower total magnetic field, thus reducing the parallel heat flux at the strike point, and expanding the wetted area at the target, which is proportional to the major radius of the strike point for otherwise similar radial extent of the divertor footprint. In turn, reducing the parallel heat flux at the divertor targets is predicted to facilitate access to divertor detachment by increasing the electron density and reducing the electron temperature. When the divertors are attached, the electron density is predicted to increase with the the square of the major radius of the strike points [23] and the electron temperature decreases with the inverse square of the strike point major radius. In low aspect ratio devices such as MAST Upgrade, the major radius of the outer strike points can be varied over a considerable range, from ~0.8m to ~1.45m within tightly baffled divertor chambers (a larger variation in the strike point major radius is possible by moving the outer strike points inward to a major radius of 0.33m, however this divertor configuration would be unbaffled, complicating comparison with other, baffled, configurations). By comparison, the conventional aspect ratio TCV tokamak can vary the major radius of the outer strike point from 0.62m to 1.06m [19], and was observed to have a modest impact on detachment access when the divertor was unbaffled, and a more pronounced effect in baffled divertor configurations [24].

Due to the low major radius of the inner strike points in low aspect ratio devices, managing heat fluxes to the inner divertors is more challenging. Therefore, MAST Upgrade typically operates in the connected double null topology to minimise the power entering the inner divertors [25].

During the design and initial operation of MAST Upgrade, extensive modelling studies were performed that predicted the Super-X configuration would offer significant benefits, including reduced divertor heat flux in the attached divertor regime [26, 27] and improved access to the detached regime [28, 26] with negligible impact on the radial plasma profiles at the mid-plane, upstream of the divertors [27]. Initial experiments in low confinement experiments [29] at low heating power confirmed these benefits of the Super-X configuration compared with a conventional divertor. The results presented here build on previous studies by performing initial experiments to study the impact of the Super-X divertor configuration in high performance H-mode pulses with significant auxiliary heating power.

The structure of this paper is as follows: a brief overview of MAST Upgrade and scenario integration issues are presented in section 2, the strategy to maximise the divertor heat flux is presented in section 3, results from initial scenario integration experiments are presented in section 4, followed by conclusions in section 5.

2. The MAST Upgrade Scenario Integration Challenge

MAST Upgrade is a low aspect ratio spherical tokamak, with typical plasma major (R) and minor (a) radii of 0.8 m and 0.5 m respectively (R/a ~ 1.6), capable of reaching a plasma current up to 2 MA (1.0 MA has been achieved to date), maximum toroidal field on axis of 0.8 T (0.72 T to date) and auxiliary heating from on-axis and off-axis neutral beam injectors, capable of injecting up to 2.5 MW each (to date, the maximum total injected power is ~3.7 MW). Typical operating scenarios are in close proximity to a connected double null topology to minimise the heat flux to the inner divertors [25] and facilitate H-mode access [30]. Initial Ohmic heated experiments to study access to detachment in conventional and Super-X divertor configurations on MAST Upgrade, could not unambigiously attach the outer divertors in the Super-X configuration, even at the lowest operating density of the device, as shown in Figure 1, corresponding to approximately 10% of the Greenwald density limit, where non-disruptive locked modes and concommitant strike point splitting were common [31]. However, this data suggests that the detachment threshold, in terms of outer mid-plane separatrix density, is substantially lower in a Super-X divertor configuration.

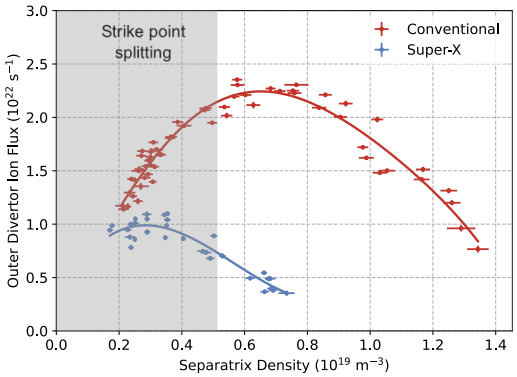

Figure 1: Outer divertor total ion flux in Ohmic heated experiments with density ramps to estimate the detachment threshold, in terms of the outer mid-plane separatrix density, in conventional (red) and Super-X (blue) divertor configurations. Detachment onset is observed when the divertor ion flux starts to decrease with increasing density mid-plane separatrix density. The approximate range of outer mid-plane separatrix density where splitting of the

outer divertor legs, indicating the onset of non-disruptive locked modes, is highlighted in grey.

The significantly lower detachment threshold in the Super-X configuration, and therefore larger operational space with detached divertors, greatly facilitates the integration of detached divertors with strong auxiliary heating and good core and edge confinement. However, it potentially poses a challenge to test the limits of scenario integration if the outer divertors remain detached in the Super-X configuration at the highest levels of heating power currently available on MAST Upgrade. This motivated the development of a plasma scenario that intentionally maximises the exhaust challenge for the divertors, to enable studies of the impact of fuelling and seeding that are typically used to moderate divertor power and particle fluxes on the core and edge/pedestal regions.

3. Maximising the Heat Flux Entering the Divertors

As explained in section 1, in future high power tokamaks, it is envisaged that the unmitigated peak divertor particle and heat fluxes will exceed material limits in the attached divertor regime. These fluxes will be moderated via fuelling and impurity seeding to promote losses of momentum and energy, which will facilitate access the detached divertor regime. In MAST Upgrade H-mode pulses with the maximum auxiliary heating available, ~3.5 MW, in the Super-X divertor configuration, in the absence of fuelling (except to fuel the plasma core) or impurity seeding, the outer divertors are typically detached.

This paper investigates an optimal plasma scenario to maximise the outer divertor target temperature was developed to maximise the probability of attaching the outer divertors, to enable studies of the impact of fuelling and/or seeding to detach them. To guide scenario development, a two-point model [32] was used to estimate the dependence of the outer divertor target temperature T_t (eV) on plasma scenario parameters in the absence of dissipation of momentum and energy in the scrape-off layer and divertor:

$$T_t = \frac{q_{\parallel}^2}{n_{e,sep}^2}\left(\frac{7 q_{\parallel} L_{\parallel}}{2\kappa_{0e}}\right)^{-4/7} \frac{2m_i}{\gamma^2 e^2} \quad (1)$$

where $n_{e,sep}$ is the electron density at the outer mid-plane (m^{-3}), $L_{\parallel}$ is the length of field lines connecting the outer mid-plane and outer divertor strike point (m), κ_{0e} is the Spitzer conductivity divided by $T^{5/2}$ (~2800 $eV^{-7/2}Wm^{-1}$) [32], m_i is the deuterium ion mass (kg), γ is the sheath heat coefficient (assumed to be ~9), e is the electron charge (C) and $q_{\parallel}$ is defined as:

$$\boldsymbol{q}_{||} = \frac{\boldsymbol{P_{SOL}}}{\boldsymbol{2\pi R_{out,mp}\lambda_{q,mp}}} \frac{\boldsymbol{B_{tot,mp}}}{\boldsymbol{B_{\theta,mp}}} \quad (2)$$

$R_{out,mp}$ is the radial position of the separatrix at the outer mid-plane (m), λ_q is the exponential decay length of the heat flux at the outer mid-plane (m), $B_{\theta,mp}$ and $B_{tot,mp}$ are the outer mid-plane poloidal and total magnetic field components respectively (T) and P_{SOL} is defined as:

$$P_{SOL} = P_{ohm} + P_{NBI,abs} - P_{rad,core} - \dot{W} \quad (3)$$

where P_{ohm} is the Ohmic heating power (W), $P_{NBI,abs}$ is the absorbed neutral beam heating power estimated by TRANSP [33] (W), $P_{rad,core}$ is the power radiated from the plasma core estimated by foil bolometers (W) [34] and $\dot{W}$ is the rate of change of plasma stored energy (W). Estimation of the two-point model parameters from experiments is described in the following sections.

3.1 Scrape-Off Layer Heat Flux Decay Length

The exponential decay length of the heat flux in the scrape-off layer (SOL), λ_q, is a key parameter to determine the heat flux density (see equation 2), of which a substantial fraction would be dissipated in detached divertor regime. In experiments, λ_q is typically estimated using spatially resolved measurements of the temperature of the divertor tiles in the attached divertor regime, where heat dissipation in the SOL and divertor is negligible, to estimate the unmitigated divertor heat flux (e.g. [35, 36, 37] on individual devices and in cross-machine studies [38]). Radial profiles of the divertor heat flux are then fit to a convolution of Gaussian and exponential profiles [39] to estimate the peak heat flux, the radial heat flux decay length λ_q and the Gaussian profile width, S, that largely determines the heat flux profile in the private flux region. A similar approach is applied here, where infrared thermography measurements of the lower outer divertor temperature profiles, and the derived heat fluxes, are routinely made. For the purposes of this study, estimates of λ_q were compared with previously published studies of its dependencies on plasma scenario parameters in [36, 38] is presented. These previous studies found a strong inverse dependence of λ_q on the poloidal field at the outer mid-plane ($\lambda_{q,Eich} \propto B_{pol,mp}^{-1.19}$, $\lambda_{q,Thornton} \propto B_{pol,mp}^{-0.68}$), and relative insensitivity to other parameters including machine size, plasma density, P_{SOL} and toroidal magnetic field. In a given device, where the plasma minor radius does not vary significantly, $B_{pol,mp}$ has a linear relationship with I_p. Measurements of λ_q in H-mode plasmas with attached outer divertors in conventional divertor configurations over a range of $0.14 \leq B_{pol,mp} \leq 0.27$, equivalent to 450 kA $\leq I_p \leq$ 1000 kA are shown in ***Figure 2***. Only measurements taken from 60% to 90% of the ELM cycle (i.e. 60 – 90% of the time between adjacent ELMs) are used in this

analysis and frames acquired during an ELM crash were excluded from the analysis. Over this period of the ELM cycle, it is expected that the pedestal parameters have stabilised after the ELMs [40]. Comparison of the total lower outer divertor power load with P_{SOL} suggests over 30% of P_{SOL} is deposited to the attached lower outer conventional divertor, which is consistent with previous results from MAST [25] and provides strong evidence that the outer divertors are attached.

The dependence of λ_q on I_p is in reasonable agreement with the previously published scalings, shown in Figure 2, however the absolute values are 30% higher than predictions from the Thornton scaling obtained on MAST [36] and 80% higher than the Eich scaling. The cause of this disagreement is unclear. The results in the following sub-sections will also show strong interdepenencies between I_p and other parameters that have been observed to more weakly influence λ_q, such as P_{SOL} and the separatrix density. However, for the purposes of this study, the dependence of λ_q on I_p is most of interest.

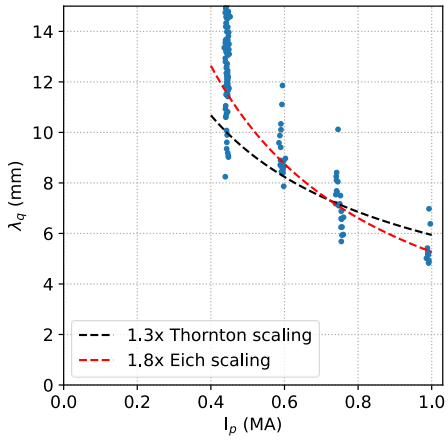

Figure 2: Measurements of λ_q in MAST-U compared with previously published scalings of its dependence on plasma current.

3.2 Separatrix Density

In H-mode, the radial profiles of electron temperature and density exhibit steep gradients in the edge pedestal region, thus making estimates of the plasma conditions at the equilbrium separatrix at the outer mid-plane highly uncertain when errors in the equilibrium reconstruction are considered. The approach adpoted in this study builds on previously reported findings [41, 42], to use a two-point model that includes the variation in magnetic field strength along field lines [43] to estimate the outer mid-plane separatrix temperature, assuming no volumetric momentum or power losses occur:

$$T_u = \left(\frac{7q_{\parallel}}{2\kappa_0}\left(\int_0^{L_{\parallel x}} \frac{B(s_{\parallel})}{B_u} ds_{\parallel} + \int_{L_{\parallel x}}^{L_{\parallel t}} (L_{\parallel t} - s_{\parallel}) \left(\frac{B(s_{\parallel})}{B(L_{\parallel t})}\right)\left(\frac{1}{L_{\parallel t} - L_{\parallel x}}\right)\right)\right)^{\frac{2}{7}} \quad (4)$$

where $L_{\parallel x}$ and $L_{\parallel t}$ are the distance along field lines from the outer mid-plane to the primary X-point, and outer divertor target respecetively (m), s is the distance along magnetic field lines and $q_{\parallel}$ is defined in equation (3). This equation is evaluated with magnetic flux and field strength estimates from EFIT++ [44, 45] equilibrium reconstruction on field lines 1cm outboard of the primary separatrix.

Radial profiles of electron temperature, T_e, and density, n_e, are measured at 1cm spatial resolution with a Thomson scattering diagnostic [40]. A Bayesian profile fitting code that includes the spatial instrument function of the finite sampling volumes in the plasma is used to fit the density and temperature profile measurements of the edge n_e and T_e profiles to a modified Tanh function to enable the pedestal separatrix density, $n_{e,sep}$, for a given separatrix electron temperature, $T_{e,sep}$, to be estimated. Typical values of $T_{e,sep}$ for 450 kA shots is 25 eV, rising to 40 eV at higher plasma current.

This approach was applied to typical H-mode scenarios in connected double null topology and conventional divertor configurations spanning a range of plasma current, 450 kA ≤ I_p ≤ 1,000 kA, toroidal field on axis 0.42 T < B_ϕ < 0.64 T, injected neutral beam power 1.1 MW < P_{NBI} < 3.5 MW, fraction of the Greenwald density limit, f_{GW}, 0.4 ≤ f_{GW} ≤ 0.6 to form a database to ascertain how the mid-plane separatrix density, $n_{e,sep}$, pedestal top density, $n_{e,ped}$ and line-average core density $\langle n_e \rangle$ vary with with I_p. These parameters were averaged over the H-mode period of each shot, only including measurements of electron temperature and density profiles taken from 60% to 95% of the ELM cycle. This database is summarised in Figure 3.

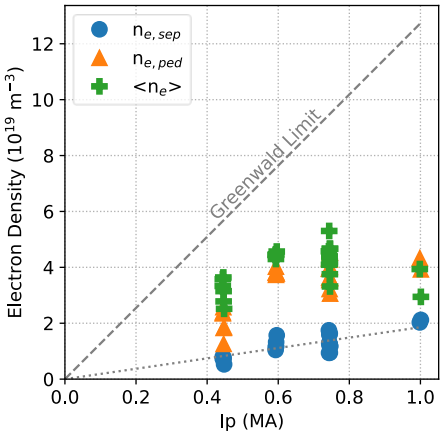

Figure 3: Dependence of the outboard mid-plane separatrix density (circles), pedestal top density (triangles) and core line-average density (crosses) and Greenwald density limit (dashed line) on plasma current in typical H-mode scenarios with attached conventional outer divertor configurations. The dotted line is a linear fit $n_{e,sep}$ (10^{19} m^{-3}) = 1.86 x Ip (MA).

Despite the large variation in the plasma scenarios in the database, there is a clear linear positive trend of $n_{e,sep}$ with I_p, as observed on other devices, such as ASDEX Upgrade [14]. There is a significant scatter in $\langle n_e \rangle$ in this database as the core line-average density steadily increases in H-mode phase of these shots. However, it is observed in all of the shots analysed that $n_{e,sep}$ amd $n_{e,ped}$ are not strongly affected as $\langle n_e \rangle$ increases in individual shots. In a given plasma scenario at constant I_p, the increase in $\langle n_e \rangle$ is due to the rising electron density near the magnetic axis, $n_{e,core}$,as shown in Figure 4, and a concommitant increase in the radial density gradient in the core.

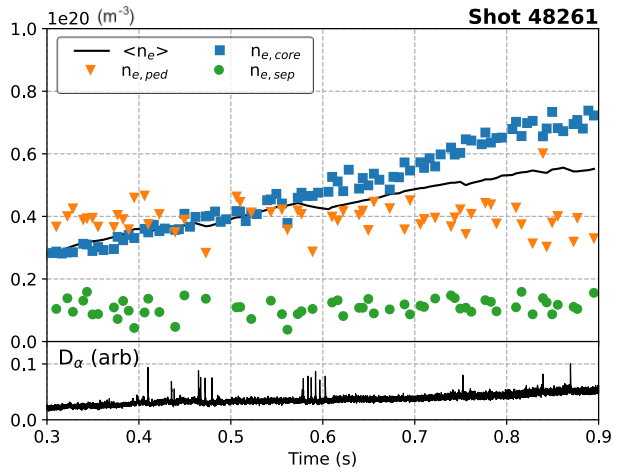

Figure 4: (top) the time variation in core line-average density ($\langle n_e \rangle$), density at the major radius of the magnetic axis ($n_{e,core}$), outer pedestal top density ($n_{e,ped}$) and outer midplane separatrix density ($n_{e,sep}$) in a typical ELMy H-mode shot, (bottom) mid-plane D_α emission, with intermittent spikes due to ELMs.

The data shown in Figure 3 does however show that both $\langle n_e \rangle$ and $n_{e,sep}$ increase with I_p, however the 600 kA scenarios generally have higher $\langle n_e \rangle$ and 1,000 kA have lower $\langle n_e \rangle$ than a simple linear trend with I_p because they were developed relatively recently, so fewer variants have been developed (reducing scatter in the data) and have not been optimised to the same extent as the other scenarios. In all of these shots, no attempts were made to reach the H-mode density limit by strongly fuelling the plasma core, although a small level (~10^{21} particles/s) of gas fuelling from a high-field side gas valve was used to moderate core MHD activity. In principle, higher fuelling could elevate $n_{e,sep}$, for example the H-mode density limit on ASDEX Upgrade has $n_{e,sep}/n_{GW}$ = 0.4-0.5 [42], compared with this database where $n_{e,sep}/n_{GW}$ = 0.15-0.2.

From this database, a simple linear regression of $n_{e,sep}$ with I_p yields $n_{e,sep}$ (10^{19} m^{-3}) = 1.86 x I_p (MA). This relation is equivalent to the separatrix density being a fraction of the Greenwald density limit, via $n_{e,sep}/n_{GW}$ = 0.15, as

$$n_{e,sep}(10^{19}\ m^{-3}) = 0.15 \times \frac{10 \times I_p(MA)}{\pi a^2} = 0.15 \times 1.25 \times 10 \times I_p(MA) = 1.875 \times I_p(MA)$$

where the typical plasma minor radius, a, is 0.5 m. This trend suggests that lower I_p scenarios are prefereable to minimise the separatrix density and hence maximise the divertor target temperature.

3.3 Absorbed Neutral Beam Power

To maximise the heat flux entering the divertors, it is important to maximise the auxiliary heating power. In MAST Upgrade, the main sources of heating are two co-current neutral beams, an on-axis beam situated at Z=0 m with a tangency radius of 0.71 m and off-axis beam at Z=0.65 m and a tangency radius of 0.8 m, both with a maximum injected power of 2.5 MW. As discussed in [46], the heating power from the on- and off-axis beams have significant differences, in particular, higher sensitivity of the heating from the off-axis beam to I_p and elongation of the plasma core. The scenarios in this study are limited to those with elongation in the range 2.0 – 2.2, which has moderate impact on the fraction of injected NBI power absorbed by the plasma. However, there is a significant variation in the aborbed NBI power when I_p is varied from 450 kA to 1,000 kA. The influence of I_p on absorbed NBI power from the on- and off-axis beams is estimated using interpretive TRANSP simulations of typical ELMy H-mode pulses studied in the preceding sections, shown in Figure 5. To help isolate the effect of I_p on NBI heating, anomalous fast ion diffusion is not applied in these simulations (for example, anomalous fast ion diffusivities of 0.5-3 m^2/s were needed to match neutron camera measurements of neutron emission to match interpretive simulations on MAST [47, 48] and MAST Upgrade [46]). This represents a best case estimate of the absorbed NBI power. Additional losses of injected NBI power due to charge-exchange interactions with main chamber neutrals are also not considered here.

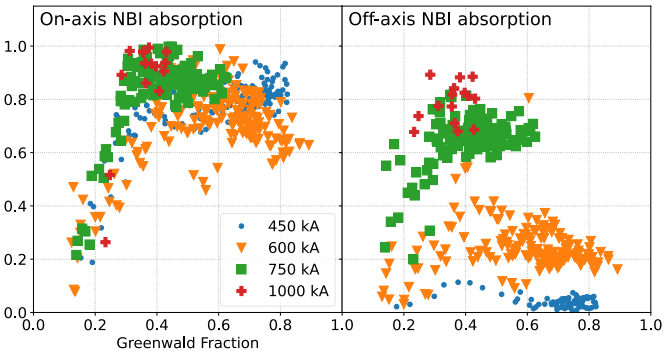

Figure 5: Estimates of the fraction of the injected neutral beam power absorbed by the plasma from the on-axis beam (left) and off-axis beam (right) as a function of the core line-average density as a fraction of the Greenwald density limit.

These TRANSP simulations show that the absorption of both beams is sensitive to the core density when $f_{GW} < 0.3$, due to increased beam shine-through at lower density. At higher core density, the absorption of the on-axis beam is relatively insensitive to I_p, compared with the scatter in the data. However, when $f_{GW} > 0.3$, the absorption of the off-axis beam is highly sensitive to I_p due to strong first-orbit lossess at lower plasma current. This suggests that scenarios with $I_p \geq 750$ kA are preferred to maximise the auxiliary heating power.

3.4 Estimation of optimal plasma parameters for scenario integration

The analyses presented in the preceding subsections provide estimates of the key plasma parameters and absorbed auxiliary heating power and their variation with plasma current, to inform the development of an optimal scenario that maximises the temperature at the outer divertor strike points, T_t. To leading order, equation (1) indicates that T_t is most sensitive to $q_{||}^2/n_{e,sep}^2$; their variation with I_p is shown in Figure 6.

The optimal I_p to maximise the outer divertor target temperature is largely determined by the varation of the absorbed off-axis neutral beam heating power at typical core line average desities, i.e. $0.4 < n_e/n_{GW} < 0.6$. There is a strong I_p dependence of the absorbed off-axis neutral beam power at $I_p \leq 750$ kA and a much weaker dependence at higher I_p. Consequently, the mid-plane parallel heat flux, $q_{||,mid}$, increases strongly with I_p at lower I_p (< 750kA) and a weaker increase at higher I_p, while the separatrix density increases linearly with I_p. This suggests that the I_p that maximises the outer divertor temperature is 750 kA.

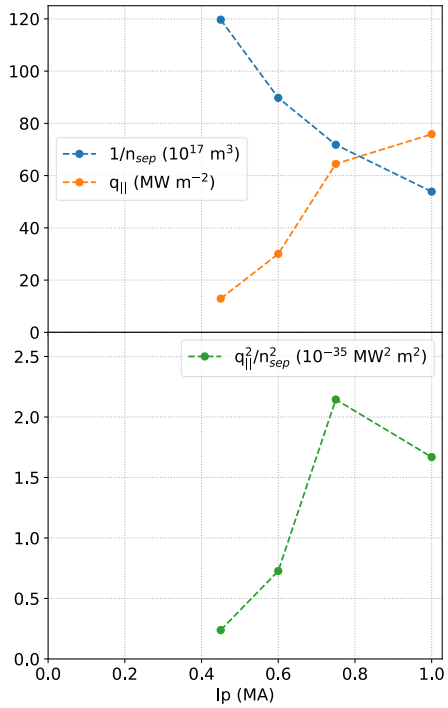

Figure 6: The variation in upstream parallel heat flux and reciprocal of the mid-plane separatrix density (above) and $q_{||}^2/n_{e,sep}^2$, where a maximum in this data is indicative of hottest outer divertor temperatures.

As discussed in the previous section, MHD instabilities can reduce fast ion confinement, as observed on MAST [49, 47, 50, 51], which vary between plasma scenarios if they cannot be avoided. Furthermore, additional auxiliary heating and current drive sources, such as a new electron Bernstein wave system that is planned for installation in 2024, will have a different density dependence on the absorbed heating power that may modify the optimum I_p for these studies in future.

4. Initial Development and Study of H-mode Scenario with a Super-X Divertor Configuration

To perform initial studies of the relative benefits of the Super-X divertor configuration on H-mode core and pedestal confinement and power exhaust, a plasma scenario was developed at $I_p = 750$ kA with 3 MW of neutral beam injection (of which, interpretive TRANSP simulations predict ~2.2 MW is absorbed) and ~0.3 MW of Ohmic heating with 0.5 MW being radiated from the plasma core (measured using resistive bolometers), suggesting that $P_{SOL} \sim 2.0$ MW. The rate of change of stored energy term in equation (3) is estimated to be negligible. The outer divertor strike points were swept from a conventional to a Super-X divertor configuration with constant core shape from 0.25s to 0.38s (shown in Figure 7), 50ms after the transition from L- to H-mode. During the H-mode phase of the shot, the plasma stored energy was 100 kJ, corresponding to an energy confinement time normalised to

the ITER H-mode scaling, $H_{98y,2}$ ~ 1.0 [52]. As the outer divertor strike points are swept to larger major radius from the conventional to the Super-X configuration, the outer strike point major radius increases from 0.76m to 1.36 m, the field line connection length from the outer mid-plane to outer divertor targets increases from 12m to 22m, poloidal flux expansion increases from 4 to 30, resulting in a reduction of the target field line incidence angle from 8^0 to 1^0. These plasmas did not feature any extrinsic impurity seeding or divertor fuelling.

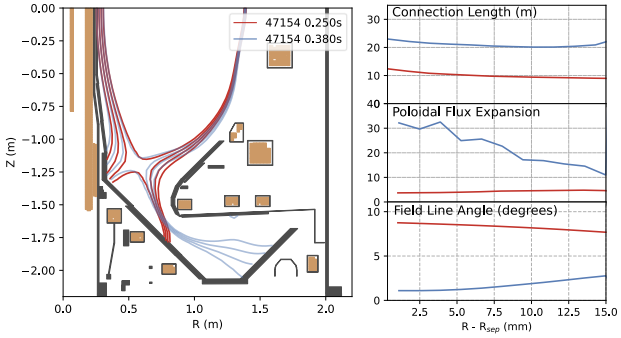

Figure 7: (Left) equilibrium reconstructions in conventional (red) and Super-X (blue) divertor configurations in shot 47154 at 0.25s and 0.38s respectively and (right) radial profiles of parallel connection length, poloidal flux expansion and field line incidence angle.

The magnetic geometry of the Super-X divertor configuration conforms to its initial description in [22], with increased strike point major radius and connection length, within the operational constraint to avoid excessive plasma power and particle fluxes to the vacuum vessel above the divertor tiles, in the gap between the divertor tiles and the divertor baffles. This was achieved by introducing secondary X-points in the divertor chamber to prevent magnetic connection of the outer mid-plane and the region above the divertor tiles in the Super-X divertor configuration via magnetic flux surfaces. This technique limits the mid-plane flux that can reach the divertor tiles to 15mm (as shown in Figure 7), or two mid-plane heat flux exponential decay lengths (see Figure 2) at this plasma current.

4.1 Impact on mid-plane profiles

In the phase of the shot where the outer strike point was swept outward, the global confinement parameters such as stored energy are well maintained, however there is a modest increase in the core line-average density from $2.9\text{x}10^{19}$ m^{-3} to $3.2\text{x}10^{19}$ m^{-3}, and an increase in the plasma stored energy from 90 kJ to 100 kJ, resulting in a commensurate increase in the normalised energy confinement time $H_{98y,2}$ from 0.8 to 1.0. The plasma gas fuelling rate was constant throughout this phase, suggesting that the increasing density trend is due to improved particle confinement in H-mode. The time variation in the mid-plane radial profiles of n_e, T_e and T_i are shown in Figure 8. The continual rise of the core line-average density is also evident in the radial profiles, most notably in the plasma core, but the electron and ion temperature profiles do not change significantly over this period.

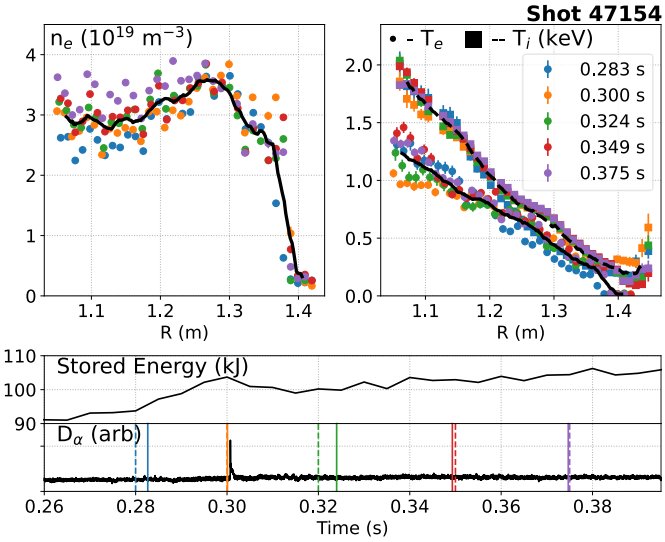

Figure 8: Mid-plane radial profiles of electron density (top left), electron and ion temperature (top right) measured using Thomson scattering and charge-exchange recombination spectroscopy (CXRS) respectively. The average of these radial profiles is overlaid in black. The plasma stored energy, estimated by equilibrium reconstruction (middle). The core plasma D_α emission and the timings of the Thomson scattering and CXRS measurements (bottom) are denoted by solid and dashed lines respectively.

These observations suggest that the changes in divertor configuration do not significantly affect the mid-plane profiles. Simple analytic 2-point models that neglect volumetric momentum and power losses [23, 53] predict a slight increase in the electron temperature at the mid-plane separatrix according to:

$$T_{e,sep} \approx \left(\frac{7q_{\parallel}L_{\parallel}}{2\kappa_0}\right)^{\frac{2}{7}}\left(\frac{ln\, f_R}{f_R-1}\right)^{2/7} \quad (5)$$

where f_R is the ratio of the major radii of the outer strike point and the separatrix at the outer mid-plane and other terms have been defined earlier. For constant $q_{\parallel}$ and taking $L_{\parallel}$ and f_R from the conventional and Super-X equilibria as presented earlier in this section, the model predicts a ~10%, or ~4-5 eV, increase in the $T_{e,sep}$. This modest increase in $T_{e,sep}$ is too small to discern from variation in the temperature profiles as the pedestal evolves and noise inherent in the profile data. Moreover, this model assumes that the outer divertor strike points are attached in both divertor configurations, which will be discussed in the following subsection.

4.2 Impact on outer divertor conditions

Sweeping the outer divertor legs out to larger major radius is expected to have a substantial impact on the plasma conditions in the divertors, in particular by reducing divertor target temperature and improving access to the detached divertor regime [22, 54, 27, 26, 55]. The effect of varying the major radius of the strike point is predicted by simplified models [23], in good agreement with predictive multi-fluid simulations in the attached divertor regime [54], that $T_{e,t} \propto \left(\frac{R_{OSP}}{R_{OMP}}\right)^{-2}$ where R_{OSP} and R_{OMP} are the major radii of the outer strike point and the separatrix at the outer mid-plane respectively. These predictions are in qualitative agreement with previous Ohmic hated L-mode experiments experiments on MAST-U [29, 56], observing that the Super-X configurations faciliates access to the detached divertor regime.

In the experiments presented here, the outer divertor strike points are swept to larger major radius using equilibrium shape controllers in feedforward control that were designed not to influence where the separatrix intersects the mid-plane at the high and low field-sides and the X-point position. The gas fuelling from the main chamber was held constant at a low level during this phase and no fuelling or seeding from the divertors was applied. As the outer strike points are swept outward, the divertor neutral compression (defined as the ratio of the measured gas pressure in the lower divertor chamber and the main chamber) is ~150 throughout, in the absence of divertor fuelling.

In the Super-X divertor configuration, there is a substantial reduction in the outer divertor ion saturation current and divertor surface heat flux profiles, as shown in Figure 9, which is a strong indicator that the outer divertors are detached. Simultaneous reductions of the outer divertor ion flux and heat flux is suggestive of substantial dissipation of plasma heat in the divertor chambers, given that the divertor parallel heat flux, $q_{\parallel,t}$ and the ion saturation current density, j^+_{sat}, are related by $q_{\parallel,t} = \gamma T_e j^+_{sat}$ [32]) that occurs when the electron temperature is sufficiently low (i.e. T_e < 1.0 eV) for frequent ion-electron recombination and potentially molecular-activated recombination processes [29, 56, 57] to occur.

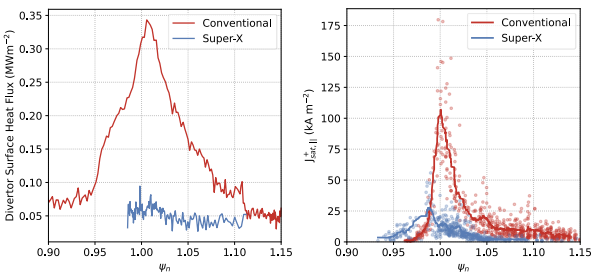

Figure 9: Divertor surface heat flux (left) and particle flux parallel to field lines (right) measured with IR thermography and Langmuir probes respectively in the conventional (red) and Super-X (blue) phases of shot 47154 as a function of normalised poloidal flux, ψ_N.

In the conventional and Super-X phases of this scan, electron pressure profiles at the mid-plane and outer divertors were measured with Thomson scattering and divertor Langmuir probes respectively, with characteristic radial profiles shown in Figure 10. The mid-plane pressure profiles are mostly unaffected by the changes in divertor configuration and there is reasonable pressure balance in the conventional divertor configuration, indicating the outer divertors are attached. Conversely, there is a significant target pressure reduction in the Super-X configuration. There is considerable scatter in the Langmuir probe inferred electron temperatures in the Super-X configuration, due to issues concerning the interpretation of the MAST-U Langmuir probe data in detached conditions [58] where the electron temperature is low. This prevents observation of a substantial reduction in the Langmuir probe inferred divertor electron temperature between the Conventional and Super-X divertor configurations. Through the plasma sheath conditions, the target pressure, p_t, is correlated with the target temperature, $T_{e,t}$, and the ion target flux j^+_{sat} via $j^+_{sat} \propto p_t/\sqrt{T_{e,t}}$, therefore $p_t \propto j^+_{sat}\sqrt{T_{e,t}}$. The strongly reduced ion target flux in the Super-X configuration is therefore consistent with the observed pressure reduction between the mid plane and the target in the Super-X, providing evidence that the Super-X is detached.

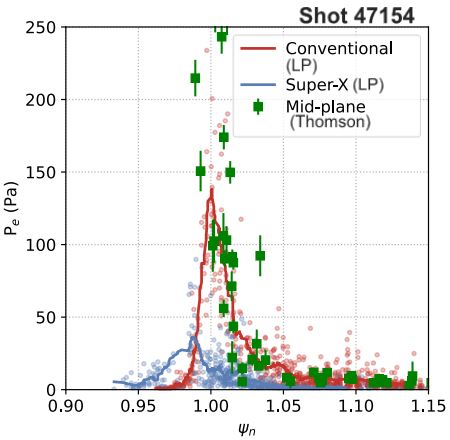

Figure 10: Mid-plane (green squares) and outer divertor electron pressure profiles multiplied by 2 in conventional (red) and Super-X (blue) divertor configurations estimated by Thomson scattering (Thomson) and Langmuir probes (LP) respectively.

5. Conclusions and Discussion

The results presented here provide first evidence that substantial reductions in the outer divertor power and particle fluxes are possible in H-mode with the Super-X divertor configuration with negligible impact on global energy

confinement and pedestal profiles in the confined plasma. These experiments were performed in a plasma scenario designed to maximise the outer divertor temperature with the aim of preventing the divertor natually detaching in the Super-X configuration to study the impact of additional fuelling and seeding to detach the divertors on the core and pedestal. This provides an important initial demonstration of the benefits of the Super-X configuration in integrating good core and pedestal confinement with plasma exhaust in MAST Upgrade.

While these initial results are very positive, there are several important open questions that need to be addressed to ascertain how they extrapolate to future devices. Most importantly, further studies at higher heating power and particle pumping are needed to attach the outer divertors in the Super-X configuration (guided by an assessment of the implications of additional heating power and particle pumping [26]). With attached outer divertors, studies of power exhaust and scenario integration can progress to deepen our understanding of the impact of fuelling and impurity seeding on exhaust and scenario integration. In turn, this will enable investigation of the degree to which impurities are retained in the divertors and whether the sensitivity of the detachment front to changes in density, radiated power and heating power is reduced in divertor configurations with high total flux expansion, predicted by theory and simulations [55, 43].

Acknowledgements

This work has been funded by the EPSRC Energy Programme [grant number EP/W006839/1]. To obtain further information on the data and models underlying this paper please contact PublicationsManager@ukaea.uk

References

[1] A. Loarte, R. Neu, Fusion. Eng. Des. **122** 256-273 (2017)
[2] R. A. Pitts et al., Nucl. Mater. Energy **20** 100696 (2019)
[3] M. Siccinio et al., Fusion Eng. Des. **176** 113047 (2022)
[4] A. W. Morris et al., Plasma Phys. Control. Fusion **64** 064002 (2022)
[5] H. Zohm et al., Fusion Eng. Des. 166 112307 (2021)
[6] A W Leonard, Plasma Phys. Control. Fusion **60** 044001 (2018)
[7] H. Raj et al., Nucl. Fusion **62** 126035 (2022)
[8] T.W. Petrie et al., Nucl. Fusion **59** 086053 (2019)
[9] L. Garzotti et al., Nucl. Fusion **59** 076037 (2019)
[10] A.M. Garofalo et al., Nucl. Fusion **57** 076037 (2017)
[11] T.W. Petrie et al., Nucl. Fusion **57** 086004 (2017)
[12] C Giroud et al., Plasma Phys. Control. Fusion **57** 035004 (2015)
[13] M. Bernert et al., Nucl. Fusion **61** 024001 (2021)
[14] A Kallenbach et al., Plasma Phys. Control. Fusion **60** 045006 (2018)
[15] T. Lunt et al., Phys. Rev. Lett. **130**, 145102 (2023)
[16] L. Wang et al., Nat Commun **12** 1365 (2021)
[17] S Coda et al., Plasma Phys. Control. Fusion 64 014004 (2022)
[18] V A Soukhanovskii Plasma Phys. Control. Fusion **59** 064005 (2017)
[19] C. Theiler et al., Nucl. Fusion **57** 072008 (2017)
[20] T. W. Morgan et al., Plasma Phys. Control. Fusion **60** 014025 (2018)
[21] W. Morris et al., IEEE Trans. on Plasma Science, 46, 5, 1217-1226 (2018)
[22] P. M. Valanju, M. Kotschenreuther, S. M. Mahajan, J. Canik, Phys. Plasmas **16** 056110 (2009)
[23] T.W. Petrie et al., Nucl. Fusion **53** 113024 (2013)
[24] C. Theiler et al., Proc. 30th IAEA Fusion Conference (2020)
[25] G De Temmerman et al., Plasma Phys. Control. Fusion **52** 095005 (2010)
[26] E. Havlíčková et al., Plasma Phys. Control. Fusion **57** 115001 (2015)
[27] E Havlíčková et al., Plasma Phys. Control. Fusion **56** 075008 (2014)
[28] A. Fil et al Nucl. Fusion **62** 096026 (2022)
[29] K. Verhaegh et al., Nucl. Fusion **63** 126023 (2023)
[30] H. Meyer et al., Plasma Phys. Control. Fusion **46** A291 (2004)
[31] T.A. Wijkamp et al., Nucl. Fusion **63** 056003 (2023)
[32] P. C. Stangeby The Plasma Boundary of Magnetic Fusion Devices (Bristol: IOP Publishing) (2000)
[33] R. Hawryluk Course on Physics of Plasma Close to Thermonuclear Conditions, Varenna, Italy (1979)
[34] J. Lovell et al., Rev. Sci. Instrum. **94**, 023509 (2023)
[35] D. Brunner et al., Nucl. Fusion **58** 094002 (2018)
[36] A J Thornton, A. Kirk Plasma Phys. Control. Fusion **56** 055008 (2014)
[37] D Silvagni et al., Plasma Phys. Control. Fusion **62** 045015 (2020)
[38] T. Eich et al., Nucl. Fusion **53** 093031 (2013)
[39] T. Eich et al., Phys. Rev. Lett. **107** 215001 (2011)
[40] R Scannell et al., Plasma Phys. Control. Fusion **55** 035013 (2013)
[41] A.W. Leonard, A.G. McLean, M.A. Makowski, P.C. Stangeby Nucl. Fusion **57** 086033 (2017)
[42] T. Eich et al., Nucl. Fusion **58** 034001 (2018)
[43] C. Cowley et al., Nucl. Fusion 62 086046 (2022)
[44] L. C. Appel et al., Comp. Phys. Comm **233** 1-17 (2018)
[45] L. Kogan et al., Proc. 48th EPS Conf. on Plasma Physics (2022)
[46] M. Cecconello et al., Plasma Phys. Control. Fusion **65** 035013 (2023)
[47] M. Turnyanskiy et al., Nucl. Fusion **53** 053016 (2013)
[48] O. M. Jones et al., Plasma Phys. Control. Fusion **57** 125009 (2015)
[49] M. Turnyanskiy et al Nucl. Fusion **49** 065002 (2009)
[50] D. Pfefferlé et al., Nucl. Fusion **54** 064020 (2014)
[51] D.L. Keeling et al., Nucl. Fusion **55** 013021 (2015)
[52] O. Kardaun, Plasma Phys. Control. Fusion **41** 429 (1999)
[53] M. Kotschenreuther et al., Nucl. Fusion **50** 035003 (2010)

[54] D Moulton et al., Plasma Phys. Control. Fusion **59** 065011 (2017)
[55] B. Lipschultz, F. I. Parra and I. H. Hutchinson, Nucl. Fusion **56** 056007 (2016)
[56] K. Verhaegh et al., Nucl. Fusion **63** 016014 (2023)
[57] K. Verhaegh et al., Nucl. Fusion **63** 076015 (2023)
[58] P. Ryan et al,. Rev. Sci. Instrum. **94**, 103501 (2023)